J Infrared Milli Terahz Waves
DOI 10.1007/s10762-011-9772-y

Electromagnetic Wave Propagation Close to Microstructures Studied by Time and Phase-Resolved THz Near-Field Imaging

Markus Walther · Andreas Bitzer

Received: 29 December 2010 / Accepted: 11 February 2011

Abstract We demonstrate microscopic mapping of electromagnetic waves close to metal microstructures with sub-ps temporal and sub-wavelength spatial resolution by pulsed THz near-field imaging. The inherent phase-sensitivity of this technique allows mapping wavefronts of propagating modes and the measured amplitude distributions provide information on field concentration and localization close to the structures. Using this approach we investigate wave propagation through a sub-wavelength aperture, as well as the formation of traveling and standing surface waves along a metal microwire.

Keywords Near-field imaging · Terahertz imaging · Microstructures · Plasmonics

1 Introduction

Manipulating light fields by their controlled interaction with metal micro- and nano-structures holds great potential for integrated and miniaturized optic technologies. The underlying principle is based on the interplay between

M. Walther (✉)
Freiburg Materials Research Center (FMF),
University of Freiburg, Stefan-Meier-Strasse 21, 79104 Freiburg, Germany
e-mail: walther@physik.uni-freiburg.de
URL: http://frhewww.physik.uni-freiburg.de/terahertz/

A. Bitzer
Institute of Applied Physics, University of Bern,
Sidlerstr. 5, 3012 Bern, Switzerland

Published online: 05 March 2011

photons and charges at the structured or unstructured metal surface [1]. As a result of this interaction localized surface modes are formed (surface plasmon-polaritons), which are bound to the interface between the metal and a dielectric (or vacuum) and, depending on their wavelength, can propagate some millimeters to meters along the surface. By specifically micro- or nano-structuring the metal, surface modes can be manipulated as well as coupled to free space. Based on this concept many novel applications, such as efficient wave-guiding, improved focusing, or enhanced spectroscopic sensitivity have been demonstrated. From an experimental perspective studies with pulsed electromagnetic radiation offer exceptional possibilities for the investigation of plasmonic effects. For example, time dependent phenomena like the formation and propagation of plasmons along the surface can be directly observed.

Over the past years pulsed THz imaging techniques have been developed, which are based on the coherent detection of electromagnetic transients [2–4]. In addition to being inherently time-resolved, these experiments allow measuring the electric field and not just light intensities, which provides information on the phase of the oscillating electromagnetic fields, allowing to directly investigate interference and resonance effects. To achieve a spatial resolution in the micrometer regime, i.e. significantly below the diffraction limit, near-field detection concepts using subwavelength apertures [5, 6], metal tips [7, 8] or point-like detectors [9–12] as near-field probes have been introduced. As a result, these experiments uniquely combine phase-sensitivity, sub-picosecond temporal and sub-wavelength spatial resolution, as required for a detailed investigation of plasmonic electromagnetic near-fields localized to micro-structured surfaces. Furthermore, owing to the long wavelength of some hundred micrometers at terahertz frequencies, structures on the subwavelength scale can easily be manufactured using conventional microfabrication techniques.

To date, a range of studies have already demonstrated the potential of THz near-field imaging for the investigation of optical near-fields close to metallic structures, such as small apertures [13–17], or microresonators and metamaterials [18–22]. Here, we extend the scope of this approach by demonstrating how particularly the intrinsic phase-sensitivity of pulsed THz near-field microscopy can be utilized to analyze the formation and propagation of electromagnetic waves close to metal micro-structures. We microscopically map THz wavefronts emanating from a subwavelength hole and propagating into free-space, as well as surface waves forming and traveling along a metallic microwire.

2 THz near-field imaging

A schematic illustration of our THz near-field microscopy system is shown in Fig. 1a. The setup is based on the coherent emission and detection of broadband THz pulses by photo-conductive antennas [12]. The output of

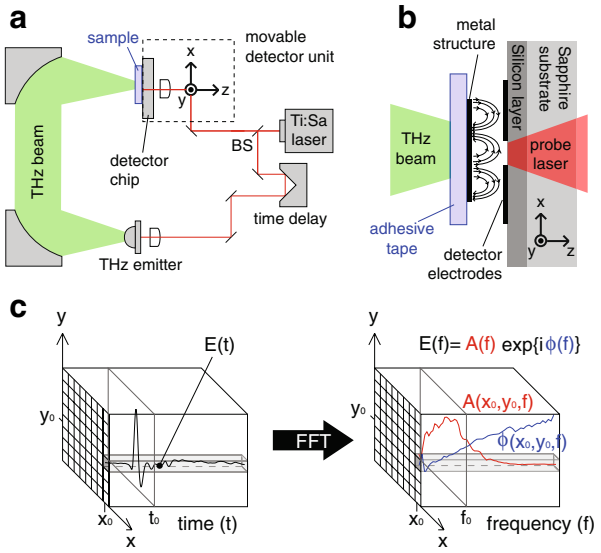

Fig. 1 **a** The THz near-field microscopy setup. **b** Close-up of a sample mounted close to the near-field detector chip. **c** At each spatial pixel a THz waveform is measured. Subsequent Fourier-transformation of the time-domain data yields frequency-dependent amplitude and phase maps.

a mode-locked Ti:sapphire laser (20 fs pulses, 800 nm, 75 MHz repetition rate) is split into an excitation beam driving the THz emitter and a detection beam gating the detector antenna. The emitted THz pulses are collimated and refocussed by a pair of off-axis paraboloidal mirrors to the position of the sample (∼1 mm spot-size). By scanning a variable delay in the excitation beam path the THz pulse incident on the sample is continuously delayed with respect to the detector gate allowing to temporally scan the THz electric field. As shown in Fig. 1b the detector is located directly behind the sample and can be moved together with the gating laser beam with micrometer precision in all three spatial directions relative to the stationary sample and the illuminating THz beam. In order to maintain the same time delay between incident THz pulse and detector gate for all spatial positions of the detector, the translation stage in the excitation beam path is moved by a commensurate distance to compensate the induced temporal delay directly during data acquisition. Our THz detector antenna consists of a H-shaped electrode structure (5 μm gap) processed on a radiation-damaged silicon-on-sapphire substrate with its electrodes facing the sample [12]. In order to gate the photo-conductive gap between the electrodes, the infrared laser beam is focussed through the sapphire substrate. Using this detector a spatial resolution on the order of 30 μm ($\lambda/10$ at 1 THz) can be achieved. Close to the sample the detector acts as near-field probe sensitive to the transverse components of the THz electric field. Rotating the polarization-sensitive detector by 90° around the beam axis between two consecutive measurements allows mapping the *x*- or the *y*-polarized field components separately, enabling in-plane vector field reconstruction as we have demonstrated previously [19–21].

As illustrated in Fig. 1c, the data obtained for one field polarization can be represented as a three-dimensional data matrix consisting of two spatial and one temporal coordinates. Plotting the data at a fixed time t_0 provides a temporal snapshot of the THz electric field distribution. Fourier transformation of the time-dependent data eventually yields spatial distributions of the amplitude and phase, which can be represented in terms of frequency-dependent amplitude and phase maps.

3 Propagating and standing waves

A spatially oscillating electric field is fully characterized by its (spatially dependent) amplitude and phase. First, we consider a plane wave traveling in positive x-direction as shown in Fig. 2a given by

$$E(x,t) = E_0 \exp\left\{ i\left(\frac{\hat{n}\omega}{c} x - \omega t \right) \right\}, \tag{1}$$

where c is the speed of light, $\hat{n}$ the refractive index of the ambient medium and ω the wave's oscillation frequency. Propagation losses in the medium are generally introduced as a non-zero imaginary part of the complex refractive index $\hat{n} = n' + in''$, resulting in an exponentially decaying amplitude as illustrated in Fig. 2a (middle, red solid line). The spatial phase of this propagating

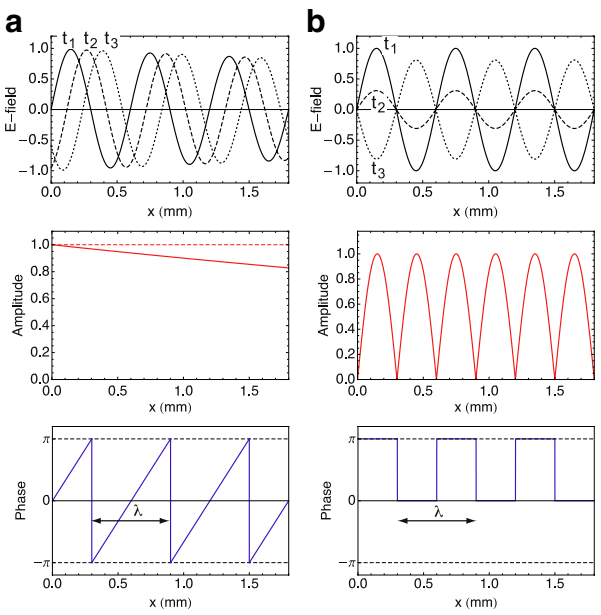

Fig. 2 Electric field of **a** a traveling wave and **b** a standing wave for three successive time steps $t_1 < t_2 < t_3$, with corresponding amplitude and phase distributions.

wave is given by $\phi(x) = \frac{n'\omega}{c}x = kx$ and corresponds to a linearly rising function with a slope equal to the wavenumber k. Figure 2a (bottom) shows the corresponding plot of the wrapped phase, i.e. with its magnitude confined to the interval $[-\pi, \pi]$. In this representation wave propagation is associated with periodic 2π-jumps as a result of the phase wrapping. These phase jumps, spatially separated by λ, represent the wavefronts of the propagating wave, with the wave-vector pointing along the gradient of the phase $\vec{k} = \nabla\phi$ [15].

Now, we consider a standing wave as illustrated in Fig. 2b. Such a stationary wave pattern is the result of two counter-propagating plane waves with same amplitude and wavelength. Hence, using the principle of superposition the electric field corresponds to

$$E(x,t) = E_0 \exp\{i(kx - \omega t)\} + E_0 \exp\{i(-kx - \omega t)\} \quad (2)$$

$$= 2E_0 \cos kx \cdot \exp\{-i\omega t\} \ . \quad (3)$$

Since now the position and time dependence are separated this wave is no longer a traveling wave. Instead, the amplitude is a function of position and oscillates between 0 (nodes) and $2E_0$ (antinodes). Two neighboring field maxima are oscillating out-of-phase which corresponds to a π-phase difference as illustrated in the phase plot.

According to these considerations it becomes apparent, that experimentally mapping amplitude and (wrapped) phase of electromagnetic waves, as possible by phase-sensitive THz imaging, allows studying wave propagation, as well as the formation of traveling and standing waves along wave-guiding structures. In the following we will give particular examples of microstructures investigated by phase-sensitive 2D THz near-field imaging.

4 Experimental results and discussion

As a first example we consider waves emerging from a subwavelength sized metallic aperture and propagating into free-space. Secondly, surface waves coupling to and propagating along a metallic microwire are studied.

4.1 Free-space wave propagation

Figure 3 shows temporal snapshots of the electric field of a terahertz pulse transmitted through a circular aperture of 300 μm diameter mechanically

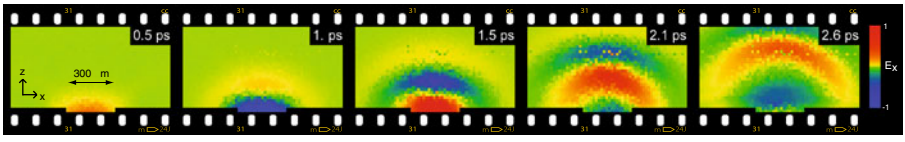

Fig. 3 Time sequence of the measured electric field distribution, E_x, of a THz pulse after transmission through a circular metallic aperture with diameter $d = 300$ μm.

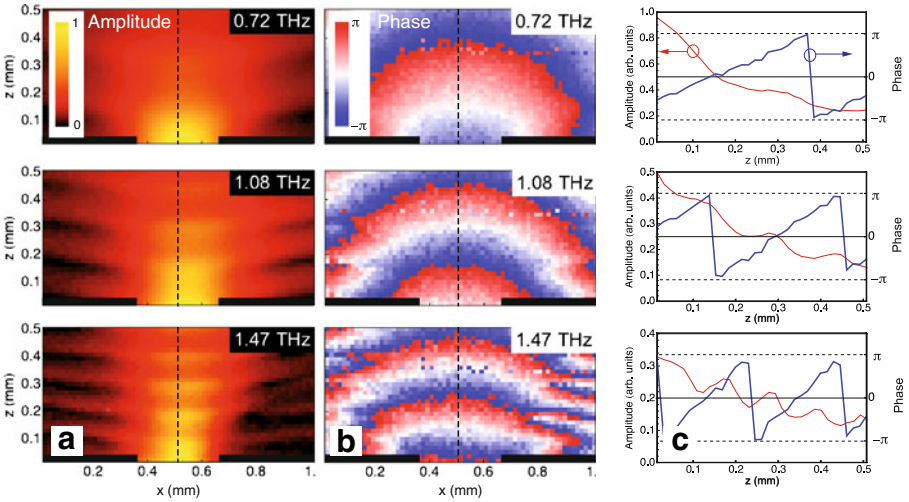

Fig. 4 **a** Amplitude and **b** phase maps of the measurement shown in Fig. 3, evaluated at three different frequencies. **c** Cross sections of amplitude and phase along the dashed lines in **a** and **b**.

drilled in a 300 μm-thick copper plate. The THz electric field was measured in a plane normal to the sample surface through the center of the hole (x, z-plane). The incident THz pulse was linearly polarized with its electric field along the x-axis and the x-component of the transmitted field E_x was measured. We observe the formation of a spherical wave radiating from the hole into free space as reported previously [15]. Fourier transformation of the time-dependent field distribution yields spectrally resolved amplitude and (wrapped) phase plots shown in Fig. 4 for three different frequencies. The amplitude plots of the x-component of the diffracted wave show maximum transmission in the forward direction with the emission pattern narrowing at higher frequencies. Note, that away from the main axis the diffracted waves contain a significant E_z contribution, which could not be measured since our detector is only sensitive to in-plane field polarizations. The oscillatory features on the sides are artifacts resulting from backreflections from the detector chip. In the wrapped phase plots the 2π phase-jumps indicate the spherical wave-fronts emanating from the hole. As discussed above, the wave vectors point along the gradient of the phase orthogonally to the phase fronts.

Cross sections of the amplitude and phase plots along the propagation axis ($x = 0.5$ mm, z) are shown in Fig. 4c. As expected, they exhibit the behavior characteristic for a traveling wave indicated in Fig. 2a, a decaying amplitude, here due to diffractive loss in the forward direction, and a linearly rising phase.

4.2 Surface guided waves

As a second example we use our approach to investigate surface waves propagating along a microwire. For this study a short piece of a cylindrical copper

wire (∼40 μm diameter) was fixed in the THz focus by using an adhesive tape as sketched in Fig. 1b. The detector was scanned in a plane ∼30 μm behind the wire in x and y-direction. Two configurations are considered: first, a pulse coupled at one wire end to the wire waveguide, and secondly, two counter-propagating pulses coupled at both opposite wire ends.

In the first case, a several millimeter long wire piece was asymmetrically positioned with one end into the approximately 1 mm wide THz focus in order to launch a pulse along the wire. We note, that for achieving such a localized excitation it is essential that the THz illumination is fixed with respect to the wire throughout the entire scan. This requires a near-field imaging setup which allows moving the detector relative to the stationary sample and stationary THz focus, instead of moving the sample. Figure 5a shows a time sequence of the x-component of the electric field measured behind the wire after illumination by a x-polarized THz field tightly focused onto one wire end. At $t = 0$ ps the illuminating field almost entirely saturates the image. On the wire end part of the field diffractively couples into a guided mode of the wire. As a result roughly 1.3 ps after excitation a THz wave packet is launched propagating along the microwire in positive x-direction. Following

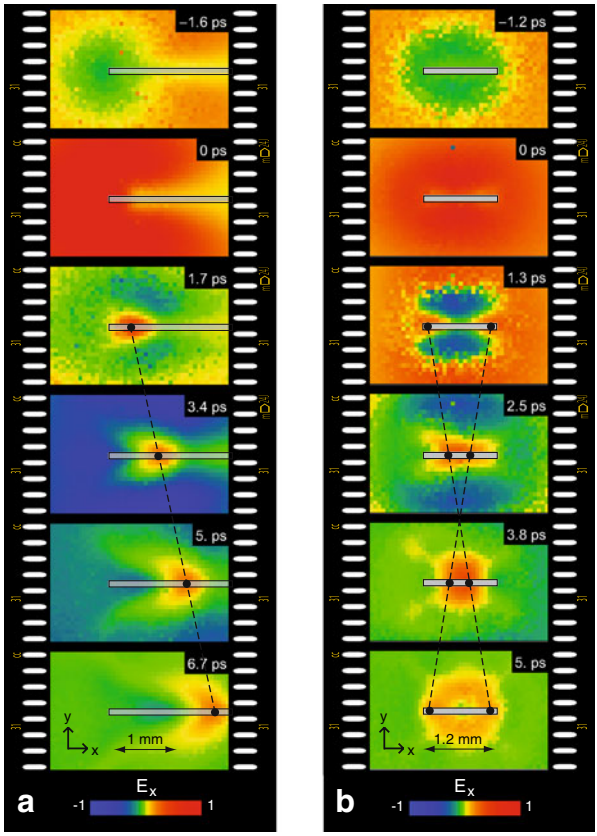

Fig. 5 Time sequence of the electric field distribution, E_x, in the x, y-plane measured ∼30 μm behind a long and a short wire piece after illumination by a THz pulse. Field pulses were launched from either only one (**a**), or both wire ends (**b**). The *dashed lines* indicate the propagation of the center of guided THz wave packets.

the propagation of the center of the wave packet (dashed line) we estimate a group velocity of $v_g = 230$ μm/ps, which matches the expected propagation velocity of c/n, where c is the speed of light in vacuum and $n = 1.3$ is the THz refractive index of the adhesive tape used to attach the wire to the sample mount. While propagating along the metal wire the field pulse spatially broadens exhibiting a tilted wavefront similar to that of the emission from a traveling wave antenna [23]. The corresponding amplitude and phase maps are shown in Fig. 6 for three almost equally spaced frequencies. Significant field concentration along the wire is observed in all amplitude maps. The corresponding wrapped phase plots exhibit 2π phase-jumps indicative for propagating modes. The cross sections of amplitude and phase along the wire axis in Fig. 6c reveal the behavior of a lossy traveling wave as shown in Fig. 2a.

As a last example a 1.2 mm long wire piece was symmetrically positioned in the center of the THz focus in order to couple two counter-propagating pulses to the wire. To ensure coupling on both ends, the THz illumination has been defocussed so that the spot size was slightly larger than the wire length. Figure 5b shows a time sequence of the measured field E_x behind the wire. In this case two pulses are launched at the wire ends propagating in opposite directions. As discussed above counter-propagating waves give rise to the formation of standing waves. The finite length of the wire (acting as resonator) results in a discrete spectrum of standing waves (resonator modes), which occur for $L = k \cdot \lambda/2$, where L is the wire length, λ the wavelength and k an integer counting the resonance order [12, 19]. Only odd resonances are

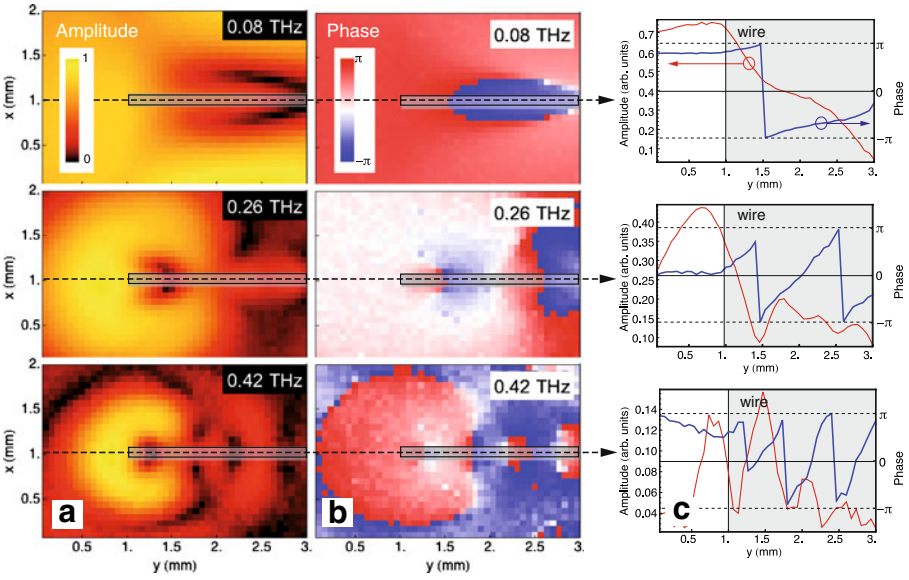

Fig. 6 **a** Amplitude and **b** phase maps of the measurement shown in Fig. 5a, evaluated at three different frequencies. **c** Cross sections of amplitude and phase along the wire axis.

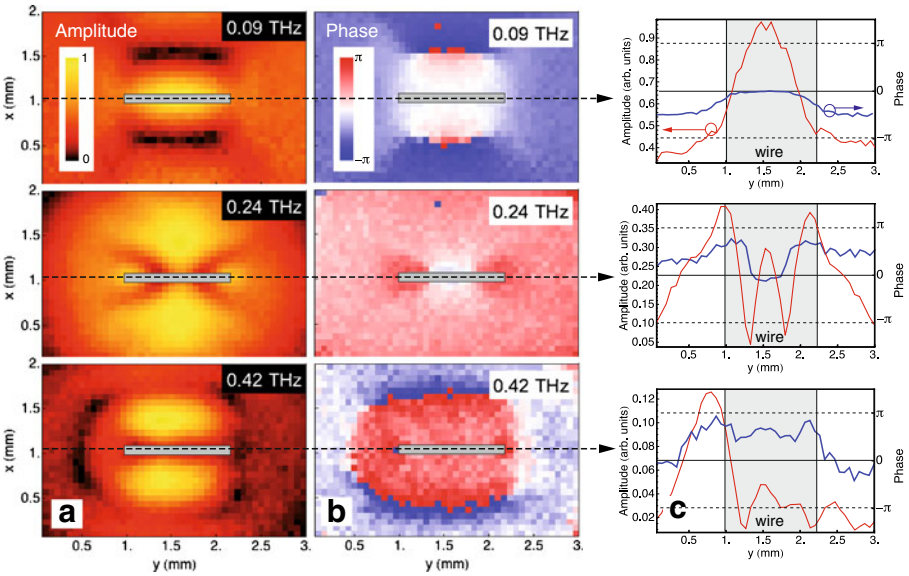

Fig. 7 **a** Amplitude and **b** phase maps of the measurement shown in Fig. 5b, evaluated at three different frequencies. **c** Cross sections of amplitude and phase along the wire axis.

associated with a non-vanishing dipole moment and can therefore be excited by an oscillating electric field. In Fig. 7a and b amplitude and phase are plotted at the odd-ordered resonances of the wire ($k = 1, 3, 5$). The amplitude shows field patterns characteristic for standing waves. Note that the pattern at 0.42 THz appears not so well pronounced due to the fact that at that frequency the THz spot size (∼1.5 mm) was barely large enough to efficiently excite both ends of the wire. The cross sections along the wire axis in Fig. 7c show a spatially oscillating amplitude with the corresponding phase switching by π between neighboring amplitude maxima, which is the characteristic behavior for a standing wave as illustrated in Fig. 2b.

5 Conclusion

In summary, we have shown that pulsed and phase-resolved THz near-field imaging can be utilized to analyze standing and traveling electromagnetic waves close to metallic microstructures. The measured amplitude distributions provide details on field concentration and localization along the structure, while the inherent phase-sensitivity of this technique allows mapping the wavefronts of propagating modes, as well as phase-flips between standing-wave lobes. Different structures and situations have been experimentally investigated, such as the THz field propagation through a subwavelength aperture and the formation of traveling and standing waves along a metallic microwire,

demonstrating the potential of this approach for the detailed characterization of electromagnetic near-fields close to artificially structured surfaces.

Acknowledgements Funding by the Deutsche Forschungsgemeinschaft (DFG) through grant No. WA 2641 and by the Baden-Württemberg Ministry for Science and Arts, Research Seed Capital (RiSC) for young researchers is gratefully acknowledged.

References

1. H. Raether, *Surface Plasmons* (Springer-Verlag, 1988).
2. D. M. Mittleman, M. Gupta, R. Neelamani, R. G. Baraniuk, J. V. Rudd, and M. Koch, "Recent advances in terahertz imaging," Appl. Phys. B **68**(6), 1085–1094 (1999).
3. W. L. Chan, J. Deibel, and D. M. Mittleman, "Imaging with terahertz radiation," Rep. Prog. Phys. **70**(8), 1325–1379 (2007).
4. M. Walther, B. M. Fischer, A. Ortner, A. Bitzer, A. Thoman, and H. Helm, "Chemical sensing and imaging with pulsed terahertz radiation," Anal. Bioanal. Chem. **397**(3), 1009–1017 (2010).
5. Q. Chen, Z. P. Jiang, G. X. Xu, and X. C. Zhang, "Near-field terahertz imaging with a dynamic aperture," Opt. Lett. **25**(15), 1122–1124 (2000).
6. S. Hunsche, M. Koch, I. Brener, and M. C. Nuss, "THz near-field imaging," Opt. Comm. **150**(1-6), 22–26 (1998).
7. H. T. Chen, R. Kersting, and G. C. Cho, "Terahertz imaging with nanometer resolution," Appl. Phys. Lett. **83**(15), 3009–3011 (2003).
8. H. T. Chen, S. Kraatz, G. C. Cho, and R. Kersting, "Identification of a resonant imaging process in apertureless near-field microscopy," Phys. Rev. Lett. **93**(26), 267401 (2004).
9. O. Mitrofanov, I. Brener, R. Harel, J. D. Wynn, L. N. Pfeiffer, K. W. West, and J. Federici, "Terahertz near-field microscopy based on a collection mode detector," Appl. Phys. Lett. **77**(22), 3496–3498 (2000).
10. O. Mitrofanov, I. Brener, M. C. Wanke, R. R. Ruel, J. D. Wynn, A. J. Bruce, and J. Federici, "Near-field microscope probe for far infrared time domain measurements," Appl. Phys. Lett. **77**(4), 591–593 (2000).
11. M. A. Seo, A. J. L. Adam, J. H. Kang, J. W. Lee, S. C. Jeoung, Q. H. Park, P. C. M. Planken, and D. S. Kim, "Fourier-transform terahertz near-field imaging of one-dimensional slit arrays: mapping of electric-field-, magnetic-field-, and Poynting vectors," Opt. Express **15**(19), 11781–11789 (2007).
12. A. Bitzer, A. Ortner, and M. Walther, "Terahertz near-field microscopy with subwavelength spatial resolution based on photoconductive antennas," Appl. Opt. **49**(19), E1–E6 (2010).
13. O. Mitrofanov, M. Lee, J. W. P. Hsu, L. N. Pfeiffer, K. W. West, J. D. Wynn, and J. F. Federici, "Terahertz pulse propagation through small apertures," Appl. Phys. Lett. **79**(7), 907–909 (2001).
14. A. J. L. Adam, J. M. Brok, M. A. Seo, K. J. Ahn, D. S. Kim, J. H. Kang, Q. H. Park, M. Nagel, and P. C. M. Planken, "Advanced terahertz electric near-field measurements at subwavelength diameter metallic apertures," Opt. Express **16**(10), 7407–7417 (2008).
15. A. Bitzer and M. Walther, "Terahertz near-field imaging of metallic subwavelength holes and hole arrays," Appl. Phys. Lett. **92**(23), 231101 (2008).
16. L. Guestin, A. J. L. Adam, J. R. Knab, M. Nagel, and P. C. M. Planken, "Influence of the dielectric substrate on the terahertz electric near-field of a hole in a metal," Opt. Express **17**(20), 17412–17425 (2009).
17. J. R. Knab, A. J. L. Adam, M. Nagel, E. Shaner, M. A. Seo, D. S. Kim, and P. C. M. Planken, "Terahertz Near-Field Vectorial Imaging of Subwavelength Apertures and Aperture Arrays," Opt. Express **17**(17), 15072–15086 (2009).
18. G. Acuna, S. F. Heucke, F. Kuchler, H. T. Chen, A. J. Taylor, and R. Kersting, "Surface plasmons in terahertz metamaterials," Opt. Express **16**(23), 18745–18751 (2008).
19. A. Bitzer, H. Merbold, A. Thoman, T. Feurer, H. Helm, and M. Walther, "Terahertz near-field imaging of electric and magnetic resonances of a planar metamaterial," Opt. Express **17**(5), 3826–3834 (2009).

20. A. Bitzer, J. Wallauer, H. Helm, H. Merbold, T. Feurer, and M. Walther, "Lattice modes mediate radiative coupling in metamaterial arrays," Opt. Express **17**(24), 22108–22113 (2009).
21. V. A. Fedotov, N. Papasimakis, E. Plum, A. Bitzer, M. Walther, P. Kuo, D. P. Tsai, and N. I. Zheludev, "Spectral Collapse in Ensembles of Metamolecules," Phys. Rev. Lett. **104**(22), 223901 (2010).
22. A. Bitzer, A. Ortner, H. Merbold, T. Feurer, and M. Walther, "Terahertz near-field microscopy of complementary planar metamaterials: Babinet's Principle," Opt. Express **19**(3), 2537–2545 (2011).
23. M. Walther, G. S. Chambers, Z. G. Liu, M. R. Freeman, and F. A. Hegmann, "Emission and detection of terahertz pulses from a metal-tip antenna," J. Opt. Soc. Am. B **22**(11), 2357–2365 (2005).